Heat capacity of, and crystal-field effects in, the RFe_2 intermetallic compounds (R = Gd, Tb, Dy, Ho, Er, Tm, and Lu)

D. J. Germano* and R. A. Butera
Department of Chemistry, University of Pittsburgh, Pittsburgh, Pennsylvania 15260
(Received 22 September 1980)

Heat capacity for RFe_2 intermetallic compounds containing the heavy rare-earth elements (R = Gd, Tb, Dy, Ho, Er, Tm, and Lu) are reported. The crystal-field contributions to the heat capacity have been evaluated and used to determine the crystal-field parameters and axis of magnetization for these compounds. The behavior of the magnetocrystalline free energies, magnetic moment, and bulk anisotropy constants as a function of temperature have been calculated. An anomaly in the heat capacity of $TmFe_2$ is reported and attributed to a spin reorientation as a function of temperature.

I. INTRODUCTION

The rare-earth metals and their intermetallic compounds have been the subject of extensive research over the past two decades. The unusual thermal and magnetic properties associated with the partially filled f shell of the rare-earth ion have made these compounds ideal materials for many experimental and theoretical investigations.[1] The RFe_2 compounds are interesting in themselves as they exhibit strong magnetic anisotropy and huge magnetostriction.[2]

The magnetic properties of the RFe_2 compounds are best described by a model in which the rare earth and iron sublattices have their spins coupled antiparallel and in which exchange between the two sublattices is an important interaction. The rare-earth–rare-earth exchange is essentially zero[3] and the antiparallel coupling between the two sublattices leads to a ferrimagnetic arrangement.[4] As a result of this antiparallel coupling and the strong crystal field interactions, the magnetostriction and magnetic anisotropy of these compounds are believed to be due primarily to the rare-earth sublattice.[2] This supposition is substantiated by the fact that the room-temperature magnetostrictions of the RFe_2 compounds, excluding nonmagnetic Lu, are at least two orders of magnitude larger than that of YFe_2 in which Y is nonmagnetic.[2]

This paper reports the results of heat-capacity measurements carried out at the University of Pittsburgh on the RFe_2 compounds: $GdFe_2$, $TbFe_2$, $DyFe_2$, $HoFe_2$, $ErFe_2$, $TmFe_2$, and $LuFe_2$. Preliminary results for the $HoFe_2$, $ErFe_2$, and $LuFe_2$ compounds have been reported by Germano *et al.*[5] and have been included in this paper for the purpose of continuity. This work is part of an ongoing heat-capacity program designed to study the RFe_2 compounds and their hydrides in an attempt to better understand the unusual properties of these compounds.

II. EXPERIMENTAL

The RFe_2 compounds, excluding $LuFe_2$, were prepared at the University of Pittsburgh by the cold boat induction heating technique.[6] The rare-earth metals were supplied by the Research Chemicals Division of the Nucor Corporation. Spectrographic analysis supplied by the manufacturer indicated that the rare-earth metals had a purity of 99.9 weight percent with respect to metallic impurities only. The iron was Johnson and Matthey Chemicals Ltd. Puratronic grade 1 rod. Spectrographic analysis by the manufacturer indicated that only silicon (1 ppm), chromium (<1 ppm) and magnesium (<1 ppm) were present as impurities. The samples used in this investigation were vacuum annealed for a period of three weeks at 800 °C. The $LuFe_2$ sample was prepared at Iowa State University by arc melting on a water cooled copper hearth. The Lu was prepared at the Ames Laboratory DOE and chemical analyses indicated that it was 99.99 at.% pure with respect to metallic impurities (H, O, C, and N concentrations were 693, 403, 233, and 25 ppm, respectively). The Fe, which was obtained from Glidden Iron, Inc., was 99.99 at.% pure with respect to metallic impurities (O, H, C, and N concentrations were 1115, 445, 37, and 25 ppm, respectively). Room temperature x-ray diffraction analysis confirmed that all samples were single phase having the cubic $MgCu_2$ structure.

The adiabatic calorimeter system used in this study has been described in detail elsewhere.[5,7] The absolute error in the data from 15 to 300 K did not exceed 1% as compared to the NBS data for Cu and benzoic acid (see Furakawa, Saka, and Reilly[7a]). Because the heat capacity of Cu is of the order of mJ/mole K below 15 K, the relative error in the experimental data was 10% to 20% in this temperature region. Therefore, the heat-capacity data from 4.2 to 15 K for the RFe_2 samples were verified by subse-

quent specific-heat measurements performed on a pulse calorimeter in this laboratory which is accurate to within 1% of the NBS Cu data in this region.

III. RESULTS AND DISCUSSION

A. General considerations

The perturbing Hamiltonians which describe the exchange and crystal-field interactions along the cubic axes of magnetization can be expressed as follows:[8]

$$\mathcal{H}^{\langle 100\rangle}=2(g_J-1)\mu_\beta\vec{H}_{\text{exch}}\cdot\vec{J}+B_4^0(O_4^0+5O_4^4)+B_6^0(O_6^0-21O_6^4)\ ,$$

$$\mathcal{H}^{\langle 110\rangle}=2(g_J-1)\mu_\beta\vec{H}_{\text{exch}}\cdot\vec{J}-\tfrac{1}{4}B_4^0(O_4^0-20O_4^2-15O_4^4)-\tfrac{13}{2}B_6^0(O_6^0+\tfrac{105}{26}O_6^2-\tfrac{105}{13}O_6^4+\tfrac{231}{26}O_6^6)\ ,$$

$$\mathcal{H}^{\langle 111\rangle}=2(g_J-1)\mu_\beta\vec{H}_{\text{exch}}\cdot\vec{J}-\tfrac{3}{2}B_4^0(O_4^0-20\sqrt{2}O_4^3)+\tfrac{16}{9}B_6^0(O_6^0+\tfrac{35}{4}\sqrt{2}O_6^3+\tfrac{77}{8}O_6^6)\ ,$$

where g_J is the Landé g factor, μ_β is the Bohr magneton, B_n^m are the crystal-field intensity parameters, and O_n^m are the Stevens operator equivalents.[8] Diagonalization of the appropriate Hamiltonian for the rare earth of interest results in a set of eigenvalues $\{E_i\}$ which can be used in the partition function:

$$Q=\sum_i g_i\exp\left(-\frac{E_i}{kT}\right)\ ,$$

where g_i is the degeneracy of energy level E_i. This partition function can be used to calculate the heat capacity, magnetic moment, and magnetocrystalline free energy for the rare-earth ion of interest.

The magnetocrystalline free energy can be calculated at any temperature using the expression

$$F=-RT\ln Q\ .$$

As it stands, this expression does not give an absolute value for the free energy because Q contains an arbitrary factor $\exp(-E_0/kT)$ and therefore, F contains an arbitrary term E_0. However, the lowest crystal field energy level determines E_0. Since each direction of magnetization has a different energy manifold, the axis of magnetization must be specified when calculating F. Using the $\langle 111\rangle$ direction as an example

$$F_{\langle 111\rangle}=E_{0\langle 111\rangle}-RT\ln Q_{\langle 111\rangle}\ .$$

The magnetization at a given temperature can also be determined using crystal-field theory. The magnetization per mole of rare-earth ion can be expressed as

$$M=N_0\sum\mu_i e^{-E_i/kT}/Q\ ,$$

where μ_i is the magnetic moment of the ith energy level. The magnetic moment per ion is given by

$$\sigma=M/(N_0\mu_\beta)\ .$$

In addition to the magnetization and magnetic moments, crystal field theory can be used to determine the bulk anisotropy constants at any temperature. For cubic symmetry, the free energy can be expressed as an expansion in α_1, α_2, and α_3, the direction cosines of the direction of magnetization with respect to the cube edges

$$F=K_0+K_1(\alpha_1^2\alpha_2^2+\alpha_2^2\alpha_3^2+\alpha_3^2\alpha_1^2)+K_2(\alpha_1^2\alpha_2^2\alpha_3^2)+\cdots\ ,$$

where K_0, K_1, and K_2 are the bulk anisotropy constants. Atzmony *et al.*[9] have shown that K_1 and K_2 can be obtained at any temperature if the free energies in the three directions of magnetization are known. The expressions relating the free energy to K_1 and K_2 are as follows:

$$K_1(T)=[4F(\vec{n}_2,T)-4F(\vec{n}_1,T)]\ ,$$

$$K_2(T)=[27F(\vec{n}_3,T)-36F(\vec{n}_2,T)+9F(\vec{n}_1,T)]\ ,$$

where $\vec{n}_1$, $\vec{n}_2$, and $\vec{n}_3$ are the unit vectors parallel to the $\langle 100\rangle$, $\langle 110\rangle$, and $\langle 111\rangle$ directions, respectively. The constants so obtained give insight into the strength of the magnetocrystalline anisotropy.

B. Determination of the heat-capacity blank

The total heat capacity of a metallic solid can be represented as

$$C_p=C_N+C_{\text{CF}}+C_M+C_E+C_L\ ,$$

where C_N, C_{CF}, C_M, C_E, and C_L are the contributions due to the nuclear hyperfine, crystal field, magnetic, electronic, and lattice contributions, respectively. The nuclear contribution has been determined by Butera *et al.*[10] to be negligible for temperatures greater than 3 K. The Curie temperatures for the $R\text{Fe}_2$ compounds are in excess of 596 K and neutron scattering studies of HoFe_2 and ErFe_2 by Koon *et al.*[3] determined that the Fe sublattice magnetization is constant over the temperature range of this study; thus it is reasonable to assume that the magnetic con-

tribution to the heat capacity will be negligible as well. The crystal-field contribution can be obtained from the experimental heat capacity of these compounds by removing the lattice and electronic contribution through the use of what is termed a heat-capacity blank. This blank is usually determined from the total heat capacity of these compounds prepared with the nonmagnetic members of the rare-earth family. Since La^{3+} and Lu^{3+} are both S state ions which do not interact with the crystalline electric field, their intermetallic compounds are ideal candidates for heat-capacity blanks. Deenadas *et al.*[11] and Inoue *et al.*[12] found that neither the $LaAl_2$ compound nor the $LuAl_2$ compound were satisfactory blanks for the entire RAl_2 series. Variation of the Debye temperature across the rare-earth series made the use of one blank inappropriate. Inoue *et al.*[12] developed a method for determination of a heat-capacity blank specific to each member of the RAl_2 series. This method used the heat capacities of the $LaAl_2$ and $LuAl_2$ samples to determine the suitable blank for the RAl_2 of interest by linear interpolation of the heat capacity as a function of the atomic weight of the rare-earth element. $LaFe_2$ does not form and an attempt to use YFe_2 as the light blank was unsuccessful due to the fact that the atomic mass of Y is much less than the rare earths and thus its heat capacity did not correlate with those of the RFe_2 series.

However, having determined the heat capacity of $LuFe_2$ throughout the temperature region, it was possible to scale the $LuFe_2$ C_p values obtained to those of $LuAl_2$. A suitable heat-capacity blank for the individual RFe_2 compounds was determined in the following manner.

According to Inoue *et al.*[12] the C_p blank for the respective RAl_2 compound at some temperature T was determined by:

$$C_p(\text{blank}) = C_p(LuAl_2) + X \ ,$$

where $X = \Delta C_p$ (atomic wt. of Lu−atomic wt. of R)/(atomic wt. of Lu−atomic wt. of La). ΔC_p in this equation is expressed as follows

$$\Delta C_p = \{C_p(LaAl_2) - T\Delta\gamma[(La-Lu)Al_2)] - C_p(LuAl_2)\} \ ,$$

where

$$\Delta\gamma[(La-Lu)Al_2] = 0.0053$$

J/mole K^2 in, and represents the difference in electronic contribution to the heat capacity between $LaAl_2$ and $LuAl_2$. Using the $LuFe_2$ C_p data contained herein, the C_p blank for any RFe_2 compound at some temperature T is

$$C_p(\text{blank } RFe_2) = C_p(LuFe_2)[C_p(\text{blank } RAl_2)/C_p(LuAl_2)] \ ,$$

where the respective C_p values are taken at said temperature T.

This approach assumes that the variation in the Debye temperatures (or lattice contributions) in the RFe_2 series is approximately the same as in the RAl_2 series. Butera *et al.*[10] determined Θ_D for many members of the RFe_2 series using β determined from low-temperature heat-capacity measurements, 1.5 to 10 K. Hungsberg *et al.*[13] determined Θ_D for $LaAl_2$ and $LuAl_2$ from heat-capacity studies but few of the remaining members of the RAl_2 have been calorimetrically studied in the low-temperature range. Therefore, accurate values of β are lacking for the other members of the series; although Inoue[14] does report approximate values of Θ_D for several RAl_2 compounds. The variation of Θ_D is found to be similar in both series; increasing with increasing atomic weight of the rare-earth metal. This behavior is also similar to that of the pure rare-earth metals.[15] The procedure used by Inoue *et al.*[12] was determined to be accurate to ±5% in the heat capacity of the rare-earth system. We estimate that the extension of this method which is used in this work would introduce the same systematic limit of ±5%.

C. $GdFe_2$

Figure 1 gives a C_p vs T plot of the experimental heat-capacity data for the $GdFe_2$ compound. The experimental data from 4.2 to 20 K were obtained from Butera *et al.*[10] because of the increased accuracy of the pulse calorimeter in this temperature region. The error bars for the data never exceed the width of the points due to the scale in Fig. 1. This is true for all subsequent C_p vs T plots.

The Gd^{3+} ion is an S-state ion and as such is not expected to interact with the crystalline electric field.[16,17] However, upon subtraction of the heat-capacity blank, there remains a definite contribution to the heat capacity, ΔC_p, as illustrated in Fig. 2. This contribution is significant, as indicated by the

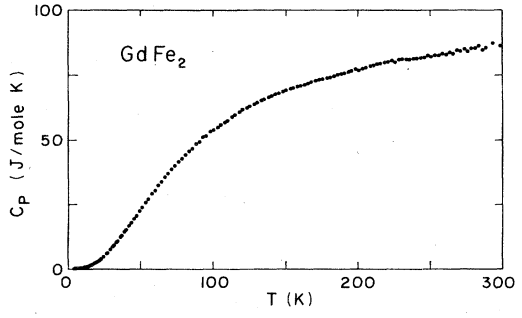

FIG. 1. Experimental heat-capacity data vs temperature for $GdFe_2$.

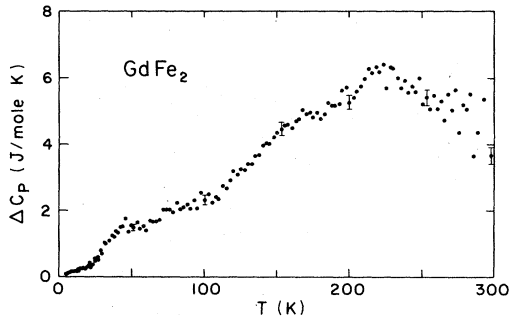

FIG. 2. ΔC_p vs temperature for $GdFe_2$.

substantial experimental excess entropy, ΔS_{expt}, obtained. In the case of the rare-earth ions, thermal excitation over the $2J+1$ levels of the ground-state results in a contribution to the entropy which can be expressed as

$$\Delta S_{\text{calc}} = R \ln(2J+1) \ ,$$

where R is the ideal gas constant. As stated before, one would not expect an interaction with the crystalline electric field in the case of the Gd^{3+} ion. However, there is a contribution to the entropy throughout the temperature region as illustrated in Fig. 3. At 300 K, $\Delta S_{\text{expt}} = 7.01$ J/mole K and $\Delta S_{\text{expt}}/R \ln(2S+1) = 0.40$.

The ΔC_p obtained for $GdAl_2$ by Thompson[18] bears a striking resemblance to that encountered in this study. Deenadas *et al.*[11] offered no explanation for this behavior and Thompson[18] attributed it to the destruction of ferromagnetism over a large temperature range. An attempt was made to fit ΔC_p by assuming that, for the case of $GdFe_2$, the degeneracy of the ground state is raised by the molecular field generated by the iron ions. However, the data could not be represented by this model.

EPR studies of the Gd^{3+} ion in many different crystalline mediums have noted splitting of the ^8S ground state due to crystal-field effects. This splitting is most likely the source of the ΔC_p in this heat-capacity study. Wybourne[17] postulated that the splitting of the Gd^{3+} ground state detected by EPR in Gd-doped $La(C_2H_5SO_4)_3 \cdot 9H_2O$ was due to two major contributions: (1) the intermediate coupling of other L,S states into the ground state; and (2) relativistic effects.

The resulting intermediate coupled states for the ground state of Gd^{3+} was expressed by Wybourne[17] as $|^8S_{7/2}\rangle = 0.987|^8_7S\rangle + 0.162|^6_7P\rangle - 0.0121|^6_7D\rangle$. The relativistic contribution results from the fact that crystal-field matrix elements between states of different spin which vanish in the nonrelativistic limit are no longer zero.[17] Chatterjee *et al.*[19] have proposed two models to describe the relativistic contribution to the crystal field.

Although the crystal-field contribution to the Gd^{3+} ground state has been ignored in previous heat-capacity studies, there is a mechanism by which the crystal field can contribute to the heat capacity of gadolinium compounds. However, simulation of this complex interaction with a computer program was beyond the scope of this study but it is hoped that the results reported within will be used to verify subsequent theoretical models.

D. $TbFe_2$

Figure 4 gives a C_p vs T plot of the experimental data for $TbFe_2$ over the temperature region 4.2 to 300 K and Fig. 5 gives a plot of ΔC_p vs T for $TbFe_2$ with the calculated best-fit curve drawn through the data. From ^{57}Fe Mossbauer measurements,[9,20] it was determined that the easy direction of magnetization of $TbFe_2$ at all temperatures is $\langle 111 \rangle$. The perturbing Hamiltonian was diagonalized with both the crystal-field interaction and exchange interaction in the $\langle 111 \rangle$ direction for a number of combinations of B_4^0, B_6^0, and H_{exch}. It must be noted at this time that the best fits for the RFe_2 compounds were verified

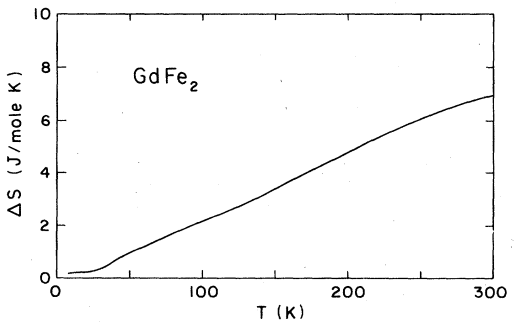

FIG. 3. Δs_{expt} vs temperature for $GdFe_2$.

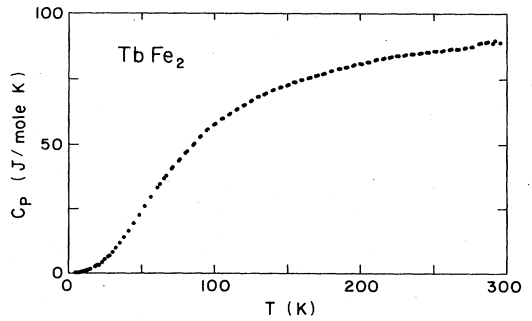

FIG. 4. Experimental heat-capacity data vs temperature for $TbFe_2$.

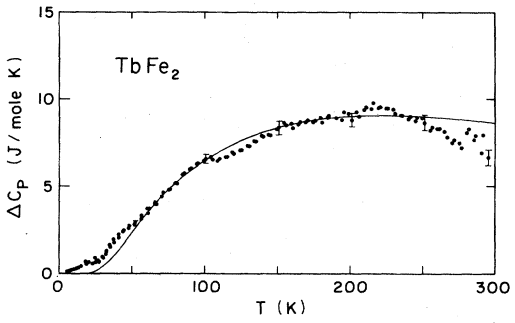

FIG. 5. ΔC_p vs temperature and calculated best fit curve for $TbFe_2$.

by attempting to fit the ΔC_p with the Hamiltonian in all three directions. The easy direction of magnetization was not assumed to be the one determined by Mössbauer spectroscopy. The best fit resulted from the following values for the crystal field parameters and H_{exch}: $B_4^0 = (1.01 \pm 0.10) \times 10^{-2}$ K, $B_6^0 = (2.00 \pm 0.20) \times 10^{-5}$ K, and $H_{\text{exch}} = 244 \pm 25$ T. The ratio of A_6^0/A_4^0 is $-0.054 a_0^{-2}$.

A_4^0 and A_6^0 are additional crystal-field parameters related to B_4^0 and B_6^0 by the following expressions:

$$A_4^0 = B_4^0/\beta_J\langle r^4\rangle \ , \quad A_6^0 = B_6^0/\gamma_J\langle r^6\rangle \ ,$$

where $\langle r^4\rangle$ and $\langle r^6\rangle$ are the fourth- and sixth-order Hartree-Fock $\langle r^n\rangle$ values tabulated for the rare-earth ions by Freeman and Watson.[21] β_J and γ_J are Steven's operators for the ion of interest as given by Lea, Leask, and Wolf.[22]

The energy level diagram resulting from this fit is illustrated in Fig. 6. The Γ values correspond to the degeneracies of the energy levels determined by Lea, Leask, and Wolf.[22] The exchange interaction of 244 T completely lifts the degeneracy of the ground-state multiplet as illustrated in Fig. 6.

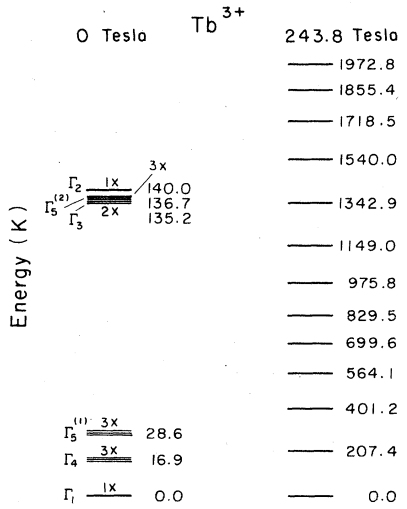

FIG. 6. Calculated energy level diagram for $TbFe_2$.

This fit is satisfactory except for the regions $T < 50$ K and $T > 250$ K. The enhanced contribution at the low end is as yet unexplained. However, the deviation at the high-temperature and is most likely due to the fact that $LuFe_2$, used in the determination of the lattice blank, has a T_c which occurs almost 100 K lower in temperature than that for $TbFe_2$.[1] A contribution to the $LuFe_2$ heat capacity from the onset of the large magnetic lambda anomaly present at the T_c would result in a high blank heat capacity in the high-temperature region of this study. As a result, when the lattice blank is subtracted from the $TbFe_2$ C_p data, ΔC_p would be low, as is the case. Due to this effect, an additional error of $\sim 1\%$ can be expected in the experimental ΔC_p and ΔS_{expt} values in this region.

The signs of B_4^0 and B_6^0 agree with the signs predicted by Bowden *et al.*[20] from ^{57}Fe Mössbauer studies. Figure 7 illustrates the behavior of the calculated magnetocrystalline free energy for $TbFe_2$ along the three possible axes of magnetization as a function of temperature. The free energy for the $\langle 111\rangle$ direction is lowest in value throughout the entire temperature region.

If the overall splitting of the energy levels given in Fig. 6 was of the order of kT, one would expect a contribution to the entropy equal to $R \ln(2J+1)$. However, at 300 K, $\Delta S_{\text{expt}}/R \ln(2J+1) = 0.62$. With an energy splitting of 1972.8 K, temperatures higher than 300 K would be required for complete population of the energy levels.

The behavior of the calculated magnetic moment of Tb^{3+} as a function of temperature is illustrated in Fig. 8. The 0-K Tb^{3+} moment, $8.96\mu_B$, is very close to the saturation value of $g_J J = 9.0\mu_B$. This value is in agreement with the value reported by Clark.[23] However, the temperature dependence of σ obtained in this study differs somewhat from experimental

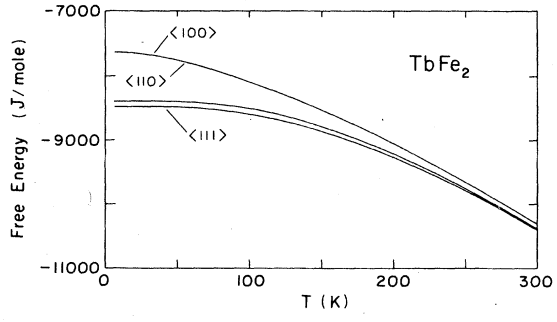

FIG. 7. Calculated magnetocrystalline free energies vs temperature for $TbFe_2$.

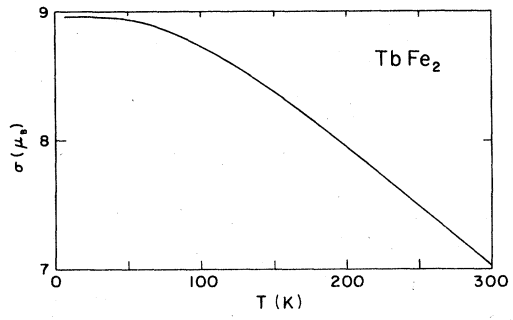

FIG. 8. Tb^{3+} calculated magnetic moment vs temperature.

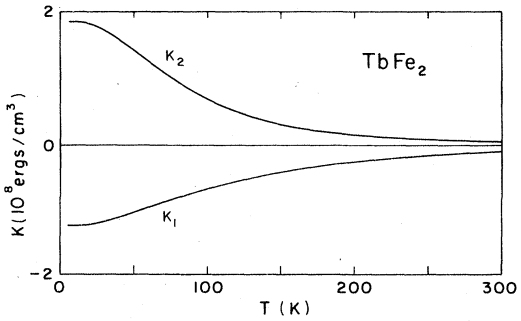

FIG. 9. Calculated bulk anisotropy constants vs temperature for $TbFe_2$.

measurements. Clark[23] reports unpublished neutron scattering results by Rhyne which establish that the room-temperature Tb^{3+} sublattice moment is 17% smaller than that at 0 K. In this study, σ at room temperature is 22% less than that at 0 K. However, the value of σ at room temperature obtained in this study is 6% lower than that reported by Clark.[23] The significance of this difference cannot be assessed as the error limits on the unpublished results are unknown.

Figure 9 gives a plot of the calculated bulk anisotropy constants, K_1 and K_2, vs T throughout the temperature range of this study. Although the anisotropy at room temperature is of more practical use, it is interesting to note that the large K_1 and K_2 values at low temperatures indicate the existence of a huge anisotropy in this region. For compounds with $K_1 < 0$, the magnetization free energy is lowest when the magnetization points along the $\langle 111 \rangle$[23] as is the case for $TbFe_2$.

Clark *et al.*[24] report that single-crystal $TbFe_2$ exhibits the largest known cubic anisotropy at room temperature. From the measured field dependence of $\sigma_{\langle 100 \rangle}$, $\sigma_{\langle 110 \rangle}$, and $\sigma_{\langle 111 \rangle}$, values for the bulk anisotropy constants were determined, $K_1 = -7.6 \times 10^7$ ergs/cm^3 and $K_2 < 2 \times 10^7$ ergs/cm^3. Because the calculated room-temperature moment from this heat-capacity study is less than that reported by Clark *et al.*[24] the calculated values for K_1 and K_2 are not expected to be as large as those reported by Clark *et al.*[24] Table I contains anisotropy constants obtained at various temperatures by several investigators. As can be seen, the smaller calculated σ does give rise to K_1 and K_2 values which are lower in value than those of Clark *et al.*[24] However, Clark[2] reports that measured magnetic moments obtained using single crystals are consistently higher in value than those of polycrystalline samples. The K_1 and K_2 values reported herein are consistent with this observation.

Atzmony *et al.*[9] calculated K_1 and K_2 at various temperatures based on ^{57}Fe Mossbauer measurements. However, they assumed that H_{exch} had a value somewhere between 149 and 238 T throughout the RFe_2 series and $H_{exch} = 223$ T was used for the calculation of K_1 and K_2 for the RFe_2 series. This value for H_{exch} differs slightly from that obtained in this case. However, the anisotropy constants calculated by Atzmony *et al.*[9] are of the same magnitude as those of this study and the behavior of K_1 and K_2 with temperature is identical. For subsequent cases in which the H_{exch} determined in this study is close to the value of 223 T assumed by Atzmony, the agreement between the bulk anisotropy constants derived

TABLE I. Selected bulk anisotropy constants for $TbFe_2$ (10^7 ergs/cm^3).

Ref.	4.2 K		80 K		300 K	
	K_1	K_2	K_1	K_2	K_1	K_2
Dariel *et al.* (20)	−63.9	7.3	−43.0	28.1	−3.85	. . .
Atzmony *et al.* (9)	−17.0	15.7	−11.8	7.7	−1.10	0.11
Clark *et al.* (21)					−7.6	< 2.0
This work	−12.6	18.5	−8.3	9.2	−1.16	0.25

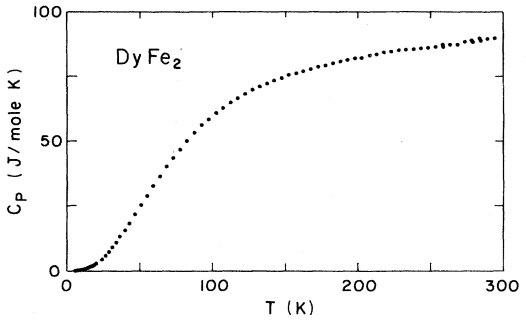

FIG. 10. Experimental heat-capacity data vs temperature for $DyFe_2$.

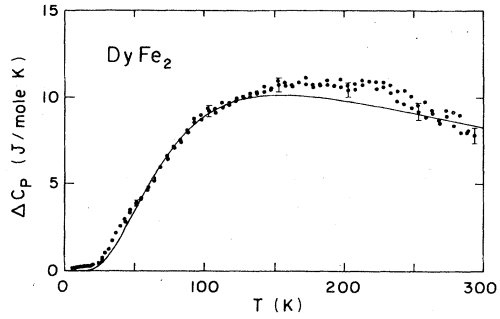

FIG. 12. ΔC_p vs temperature and calculated best fit curve for $DyFe_2$.

from Mössbauer spectrographic measurements and this work is very good.

Those values for K_1 and K_2 reported by Dariel *et al.*[25] are high compared to this work. These values were calculated based on magnetization and torque measurements by Clark *et al.*[26] on single crystal $ErFe_2$. The room temperature K_1 obtained by Clark *et al.*[26] -0.33×10^7 ergs/cm^3, is quite high and as a result, the calculated values of K_1 and K_2 of Dariel *et al.*[25] for the RFe_2 series are consistently higher than those of Atzmony *et al.*[9] and this work.

E. $DyFe_2$

A plot of the experimental C_p vs T data for $DyFe_2$ is given in Fig. 10. Scatter in the data is within experimental error limits throughout the temperature region.

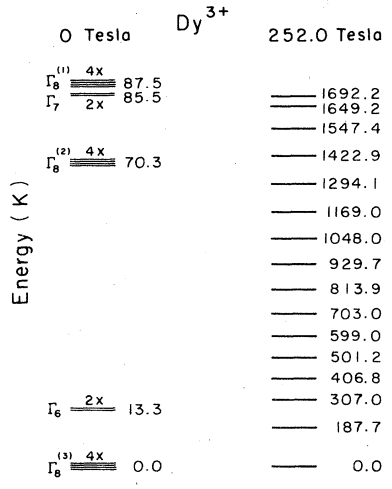

FIG. 11. Calculated energy level diagram for $DyFe_2$.

The easy direction of magnetization for $DyFe_2$ has been determined by ^{57}Fe Mössbauer measurements[9,20] to be $\langle 100\rangle$. The appropriate fit parameters obtained in this study are as follows:

$$B_4^0 = (-2.40 \pm 0.20)\times10^{-3}\ \text{K}\ ,$$

$$B_6^0 = (-6.93 \pm 0.60)\times10^{-6}\ \text{K}\ ,$$

$$H_{\text{exch}} = 252 \pm 25\ \text{T}\ .$$

The ratio of A_6^0/A_4^0 is $-0.043a_0^{-2}$ in this case and the energy level diagram resulting from the best fit is given in Fig. 11.

The greatest deviation from the experimental ΔC_p data, Fig. 12, is found in the calculated fit between 150 and 250 K. The fact that the experimental data is high in only this region tends to rule out contributions which increase linearly with temperature. The downturn in the data at the high end cannot be attributed to the disparate Curie temperatures of $LuFe_2$ and $DyFe_2$ as they differ by only 28 K. As a result, this enhancement in the ΔC_p between 150 and 250 K is as yet unexplained.

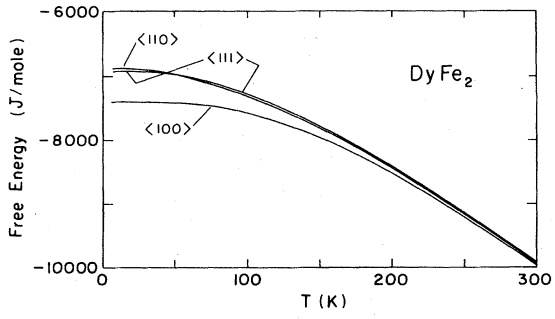

FIG. 13. Calculated magnetocrystalline free energies vs temperature for $DyFe_2$.

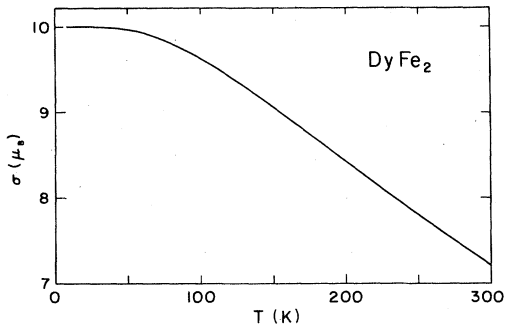

FIG. 14. Dy^{3+} calculated magnetic moment vs temperature.

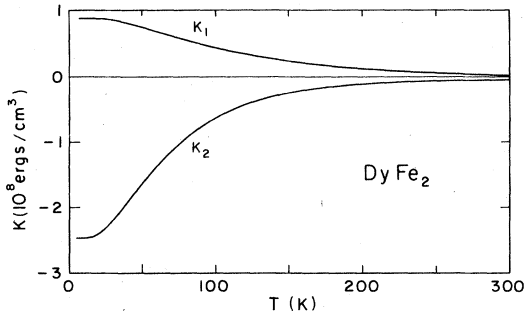

FIG. 15. Calculated bulk anisotropy constants vs temperature for $DyFe_2$.

The prediction by Bowden *et al.*[20] that the signs of B_4^0 and B_6^0 would be negative is in agreement with the results of this study. From Fig. 13, it can be seen that the calculated magnetocrystalline free energy in the ⟨100⟩ direction is lowest in value throughout the temperature range. ^{57}Fe Mossbauer studies[9,20] are in agreement with this result.

$\Delta S_{\text{expt}}/R \ln(2J+1) = 0.74$ for $DyFe_2$ and because the overall splitting of the energy levels in $DyFe_2$ is ~300 K less in energy than that of $TbFe_2$, one would expect a larger contribution to the entropy in $DyFe_2$, as is the case.

Figure 14 gives the behavior of the calculated Dy^{3+} moment as a function of temperature. The 0-K moment, $9.99\mu_B$, is essentially equal to the free ion value, $10\mu_B$, which is in agreement with Clark;[23] this moment is reduced by 28% at 300 K. The behavior of the moment as a function of temperature agrees with the magnetization data of Burzo[27] and the neutron-diffraction work of Rhyne as reported by Clark.[23] Figure 15 gives a plot of K_1 and K_2 vs T. K_1 remains greater than zero throughout the temperature range, thus verifying that the ⟨100⟩ direction is parallel to the easy axis of magnetization. For reasons previously described in the case of $TbFe_2$, the anisotropy constants obtained by Atzmony *et al.*[9] are in better agreement with those reported in this work (Table II).

F. $HoFe_2$

The experimental data for $HoFe_2$ as a function of temperature are illustrated in Fig. 16.

The crystal-field contribution to the heat capacity of $HoFe_2$ is substantial, as illustrated by the plot of ΔC_p vs T given in Fig. 17. ^{57}Fe Mössbauer measurements by Atzmony *et al.*[9] and Bowden *et al.*[20] have determined that the easy axis of magnetization for $HoFe_2$ at all temperatures is ⟨100⟩. However, Atzmony had suggested in a later paper that the easy axis is rotated slightly away from ⟨100⟩ at 10 K.[28] Neutron-diffraction studies by Rhyne *et al.*[29] also indicated the possible existence of a transition in this region though they admit that the effect was subtle and conclusions based on the result would be premature. The heat-capacity data reported herein do not exhibit the anomaly expected at 10 K if rotation oc-

TABLE II. Selected bulk anisotropy constants for $DyFe_2$ (10^7 ergs/cm^3).

Ref.	4.2 K K_1	4.2 K K_2	80 K K_1	80 K K_2	300 K K_1	300 K K_2
Dariel *et al.* (20)	83.5	−252.6	45.0	−53.2	2.69	· · ·
Atzmony *et al.* (9)	25.1	−60.6	13.3	−18.7	0.72	−0.15
Clark *et al.* (21)					2	· · ·
This work	8.8	−24.6	5.4	−9.1	0.50	−0.17

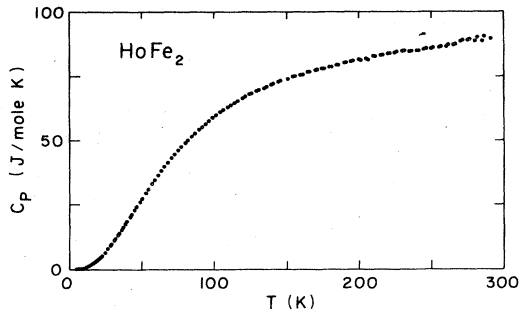

FIG. 16. Experimental heat-capacity data vs temperature for $HoFe_2$.

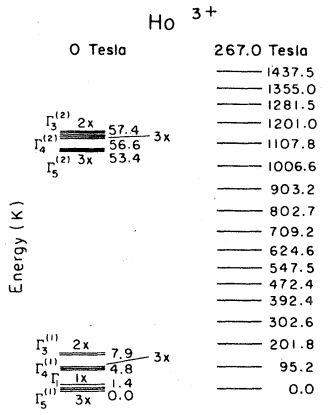

FIG. 18. Calculated energy level diagram for $HoFe_2$.

curs, leading to the conclusions that the ⟨100⟩ axis is easy throughout the temperature region of this study.

The Hamiltonian containing the exchange interaction and crystal-field interaction in the ⟨100⟩ direction of magnetization for Ho^{3+} was diagonalized for a number of combinations of B_4^0, B_6^0, and H_{exch}. The ΔC_p curve was evaluated for the energy levels obtained from the diagonalization and the best fit resulted from the following values of B_4^0, B_6^0, and H_{exch}:

$$B_4^0 = (-9.26 \pm 0.90) \times 10^{-4} \text{ K} ,$$

$$B_6^0 = (5.10 \pm 0.50) \times 10^{-6} \text{ K} ,$$

$$H_{\text{exch}} = 267 \pm 25 \text{ T} .$$

The ratio A_6^0/A_4^0 is $-0.038\ a_0^{-2}$ in this case.

The energy level diagram derived from this fit is illustrated in Fig. 18. The large H_{exch} of 267 T, completely lifts the degeneracy of the ground-state multiplet.

This calculated fit is within experimental error limits until ~100 K, above which the fit deviates low. It is highly unlikely that this contribution is due to spin waves since Eg in $HoFe_2$ (Ref. 29) has a higher value than that of $ErFe_2$ (Ref. 30) which, as will be seen later, does not exhibit an extra contribution to ΔC_p. On the basis of the respective values of Eg, a larger, if any, spin-wave contribution would have been expected in $ErFe_2$. The source of this deviation is as yet unexplained.

The parameters, B_4^0, B_6^0, and H_{exch}, used for the best fit are in direct agreement with those obtained from neutron-diffraction studies by Rhyne *et al.*[29] The ratio of A_6^0/A_4^0 agrees with the results of spin reorientation studies[28] and correlates with most of the members of the RFe_2 series.

At 300 K, $\Delta S_{\text{expt}}/R \ln(2J+1)$ is 0.85 for $HoFe_2$, again indicating that higher temperatures are necessary to populate the entire manifold.

Figure 19 illustrates the behavior of the calculated magnetocrystalline free energies as a function of temperature. The free energy for the ⟨100⟩ direction has the lowest value throughout the temperature region.

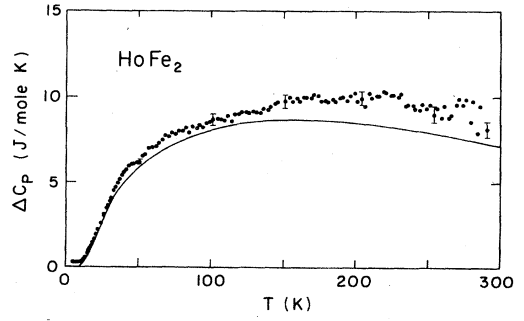

FIG. 17. ΔC_p vs temperature and calculated best fit curve for $HoFe_2$.

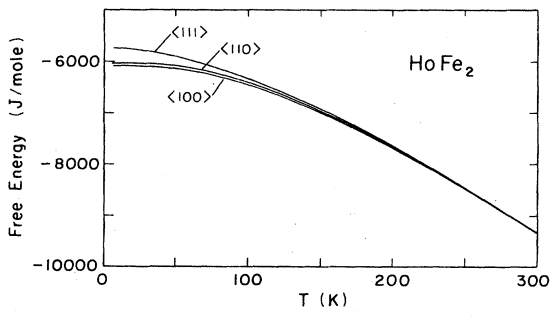

FIG. 19. Calculated magnetocrystalline free energies vs temperature for $HoFe_2$.

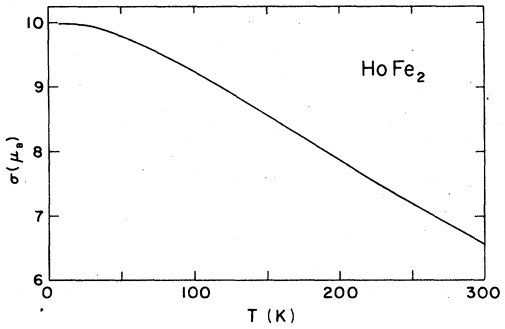

FIG. 20. Ho^{3+} calculated magnetic moment vs temperature for $HoFe_2$.

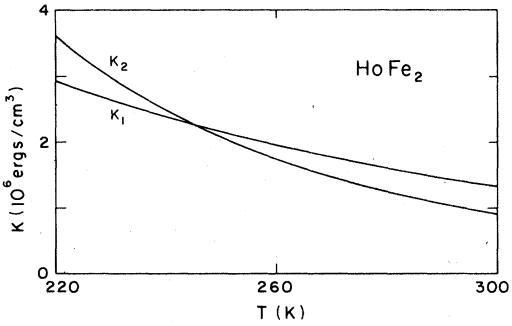

FIG. 22. Magnification of region in which the bulk anisotropy constants cross.

The behavior of the calculated Ho^{3+} magnetic moment as a function of T can be found in Fig. 20. At 0 K, σ is essentially equal to the free ion value; $9.98\mu_B$ as compared to $g_J J = 10\mu_B$. This value agrees with the moment reported by Rhyne *et al.*[29] and the temperature dependence is the same as reported by Clark.[23] At room temperature, only 66% of the calculated moment at 0 K remains.

The calculated bulk anisotropy constants have been plotted as a function of temperature in Figs. 21 and 22. Figure 22 gives a magnification of the region $220 \leq T \leq 300$ K in which the K_1 and K_2 curves cross at ~ 245 K. This type of behavior is noted by Dariel *et al.*[25] but the crossover is reported at ~ 200 K.

The K_1 and K_2 values at various temperatures as reported by Dariel *et al.*[25] and Atzmony *et al.*[9] along with those from this work can be found in Table III. The variation of K_1 and K_2 with temperature is essentially the same for the three investigations. Once again, the calculated values of K_1 and K_2 from this work are in better agreement with those reported by Atzmony *et al.*[9]

G. $ErFe_2$

Figure 23 gives a plot of C_p vs T for $ErFe_2$. The easy axis of magnetization for $ErFe_2$ at all temperatures is $\langle 111 \rangle$.[3,9,20] Therefore, the best fit to ΔC_p, Fig. 24, resulted from the diagonalization of the perturbing Hamiltonian with the exchange and crystal-field interactions in the $\langle 111 \rangle$ direction. The best fit combination of parameters is as follows:

$$B_4^0 = (1.94 \pm 0.19) \times 10^{-3} \text{ K} ,$$

$$B_6^0 = (-1.20 \pm 0.30) \times 10^{-5} \text{ K} ,$$

$$H_{\text{exch}} = 233 \pm 25 \text{ T} .$$

A value of $-0.037\ a_0^{-2}$ was calculated for A_6^0/A_4^0 and the energy level diagram which resulted in the best fit ΔC_p is illustrated in Fig. 25.

The ΔC_p fit to the experimental data is excellent. Except for the slight bump in the data between 220 and 250 K, the entire fit is within experimental error limits. This slight deviation is as yet unexplained.

The values of B_4^0, B_6^0, and H_{exch} reported are in

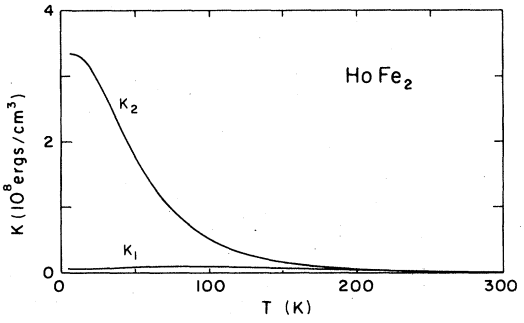

FIG. 21. Calculated bulk anisotropy constants vs temperature for $HoFe_2$.

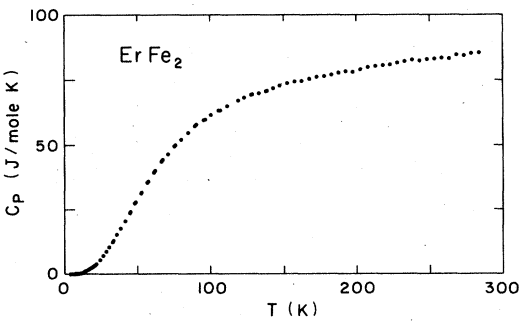

FIG. 23. Experimental heat-capacity data vs temperature for $ErFe_2$.

TABLE III. Selected bulk anisotropy constants for $HoFe_2$ (10^7 ergs/cm^3).

Ref.	4.2 K K_1	4.2 K K_2	80 K K_1	80 K K_2	300 K K_1	300 K K_2
Dariel *et al.* (20)	4.9	334.0	7.9	61.0	0.66	. . .
Atzmony *et al.* (9)	2.0	117.3	3.3	20.1	0.20	0.08
This work	0.6	33.3	1.0	8.5	0.13	0.09

direct agreement with those obtained from the neutron-diffraction studies of Koon *et al.*[3] The ratio of A_6^0/A_4^0 is in agreement with that expected for the RFe compounds.

At 300 K, $\Delta S_{\text{expt}}/R \ln(2J+1) = 0.85$. This result is the same as that for $HoFe_2$ although one would expect a difference in the ΔS_{expt} for the two compounds due to the fact that the overall splitting of the energy manifold is ~ 400 K less in $ErFe_2$. In the case of $HoFe_2$, there appears to be an extra contribution to the heat capacity which is not removed by the lattice blank, resulting in an anomalously high $\Delta C_{p_{\text{expt}}}$. This would account for the discrepancy noted in ΔS_{expt}.

The calculated free energies for $ErFe_2$ as a function of temperature are given in Fig. 26. The free energy for the $\langle 111 \rangle$ direction is lowest at all temperatures and the $\langle 111 \rangle$ direction is parallel to the easy axis of magnetization. This is in agreement with Mössbauer[9,20] and neutron-diffraction results.[3]

The calculated Er^{3+} moment at 0 K is $8.99\mu_B$ which is essentially equal to $g_J J = 9.0\mu_B$ and is in agreement with the neutron-diffraction work of Koon *et al.*[3] The behavior of σ as a function of temperature, Fig. 27, is similar to that found by Rhyne as reported by Clark.[23] Clark[23] reports that the room-temperature moment for Er^{3+} is $\sim 50\%$ less than at 0 K which is in agreement with this work.

Figure 28 gives a plot of the calculated K_1 and K_2 vs T for $ErFe_2$. A magnification of the temperature region from 100 to 300 K, Fig. 29, reveals that K_1 and K_2 cross at approximately 140 K. This crossover occurs in the calculated values of Dariel *et al.*[25] at ~ 150 K.

The values of K_1 and K_2 reported by Clark *et al.*[24] are higher than those calculated in this work (Table IV). However, there is better agreement than in the case of $TbFe_2$. Since Dariel *et al.*[25] based their calculations on the $ErFe_2$ data of Clark *et al.*[24] the K_1 and K_2 values reported by the two investigators will be identical.

H. $TmFe_2$

A plot of the experimental C_p vs T data for $TmFe_2$ is given in Fig. 30. Scatter in the data is within experimental error limits throughout the temperature region. However, there is a variance in curvature in the data at ~ 55 K indicating the presence of a possible anomaly.

Figure 31 gives the ΔC_p vs T curve for $TmFe_2$ throughout the temperature region. The anomaly noted in Fig. 30 is a rounded transition occurring at ~ 55 K. This anomaly has not been noted in ^{57}Fe

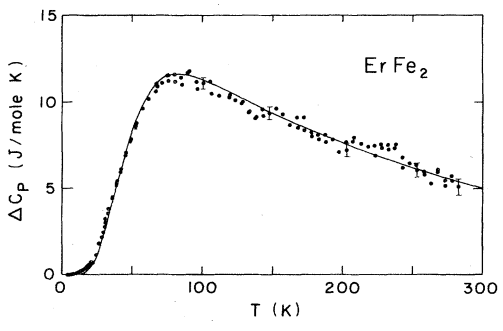

FIG. 24. ΔC_p vs temperature and calculated best fit curve for $ErFe_2$.

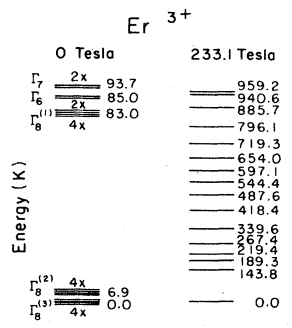

FIG. 25. Calculated energy level diagram for $ErFe_2$.

TABLE IV. Selected bulk anisotropy constants for $ErFe_2$ (10^7 ergs/cm^3).

Ref.	4.2 K		80 K		300 K	
	K_1	K_2	K_1	K_2	K_1	K_2
Dariel *et al.* (20)	−21.3	−294.4	−13.5	−32.2	−0.33	. . .
Atzmony *et al.* (9)	−3.9	−89.6	−2.9	−8.6	−0.08	−0.02
Clark *et al.* (21)					−0.33	−0.09
This work	−3.4	−28.7	−1.8	−4.4	−0.07	−0.02

TABLE V. Selected bulk anisotropy constants for $TmFe_2$ (10^7 ergs/cm^3).

Ref.	4.2 K		80 K		300 K	
	K_1	K_2	K_1	K_2	K_1	K_2
Dariel *et al.* (20)	−43.7	35.0	−8.9	1.8	−0.12	. . .
Atzmony *et al.* (9)	−19.3	45.4	−2.2	1.2	−0.02	0.00
This work	−5.9	17.8	−1.0	1.1	−0.02	0.00

TABLE VI. Summary of heat-capacity results.

Compound	B_4^0 (10^{-3}) (K)	B_6^0 (10^{-6}) (K)	H_{exch} (T)	$\frac{\Delta S_{expt}}{\Delta S_{calc}}$	Calculated rare-earth-ion 0 K σ (μ_B)	Calculated (300 K) (10^7 ergs/cm^3) K_1	K_2	Direction parallel to easy axis
$GdFe_2$				0.40				
$TbFe_2$	10.1	20.00	244	0.62	8.96	−1.2	0.26	⟨111⟩
$DyFe_2$	−2.40	−6.93	252	0.74	9.99	0.50	−0.17	⟨100⟩
$HoFe_2$	−0.93	5.10	267	0.85	9.98	0.13	0.09	⟨100⟩
$ErFe_2$	1.94	−12.00	233	0.85	8.99	−0.07	−0.02	⟨111⟩
$TmFe_2$	5.46	35.40	245	0.97	6.92	−0.02	0.00	$T \lesssim 55$ K ⟨110⟩ $T \gtrsim 55$K ⟨111⟩

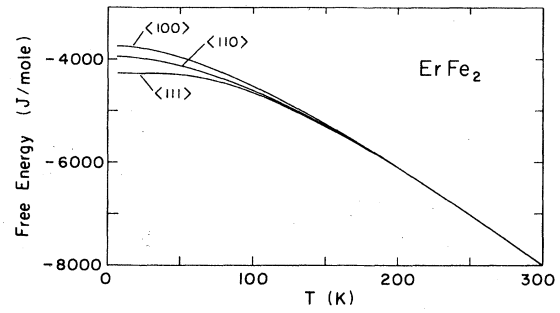

FIG. 26. Calculated magnetocrystalline free energies vs temperature for $ErFe_2$.

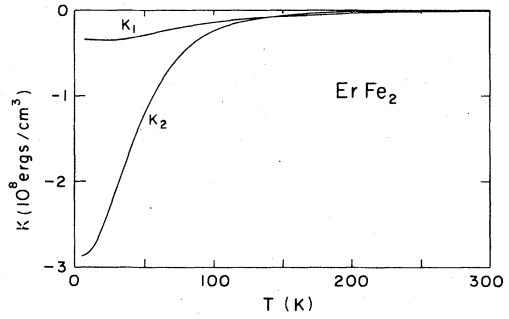

FIG. 28. Calculated bulk anisotropy constants vs temperature for $ErFe_2$.

Mössbauer studies[9,20,31] or in the unpublished neutron-diffraction studies of Rhyne.[23] From ^{57}Fe Mossbauer measurements at 4.2, 77, and 300 K, Atzmony *et al.*[9] concluded that the easy direction of magnetization for $TmFe_2$ is $\langle 111 \rangle$, thus verifying the 77-K measurement of Bowden *et al.*[20] Attempts to fit the general shape of the ΔC_p curve with the $\langle 111 \rangle$ direction of magnetization throughout the temperature range were not successful. On the other hand, the ΔC_p curve was best described by diagonalization of the perturbing Hamiltonian in two directions of magnetization. When the easy axis of magnetization varies with temperature, the compound is said to have undergone spin reorientation of the transition[28] This phenomenon occurs in many of the $R_{1-x}R'_xFe_2$ compounds[2] and in the Laves phase $HoAl_2$ compound.[32]

Theory predicts that a spin reorientation transition should be first order.[9] The transition in ΔC_p is not the type indicative of a first-order process and the continuity in the data throughout the transition suggests a cooperative mechanism. However, the familiar second-order lambda anomaly is missing and it has been replaced by a rounded curvature for reasons yet unknown. However, ^{57}Fe Mössbauer studies[9] have revealed intermediate spectra in the transition region of spin reorientation compounds which suggests that the transition is not first order. In addition, as will be seen, the calculated magnetocrystalline free energies for $TmFe_2$ in the $\langle 111 \rangle$ and $\langle 110 \rangle$ direction cross almost tangentially suggesting the possibility that the anomaly is either a smeared out first-order transition or a cooperative effect of some sort.

The most likely cause of such a transition would be an impurity in the $TmFe_2$ sample, such as an oxide. Westrum *et al.*[33] and Justice *et al.*[34,35] have measured the C_p of the R_2O_3 oxides and found the heat capacities at ~ 55 K to be on the order of 10 to 25 J/mole K. However, the heat capacity of Tm_2O_3 does not exhibit a transition at or near ~ 55 K which could account for the anomaly noted in this work.[35] In addition, x-ray analysis did not detect any oxides in the sample thereby ruling out their contribution to the heat capacity as a viable explanation.

Neutron-diffraction results are needed before the true nature of this anomaly is understood. Its presence in our data conflicts with the ^{57}Fe Mössbauer

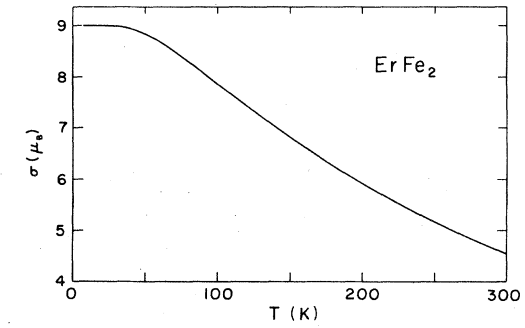

FIG. 27. Er^{3+} calculated magnetic moment vs temperature for $ErFe_2$.

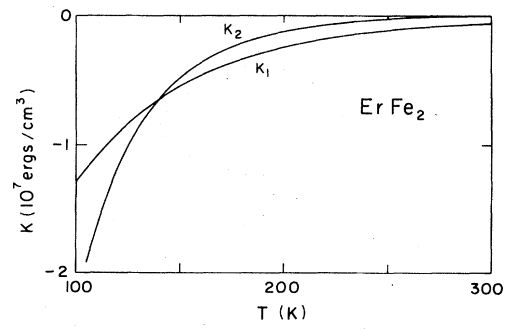

FIG. 29. Magnification of region in which the bulk anisotropy constants cross.

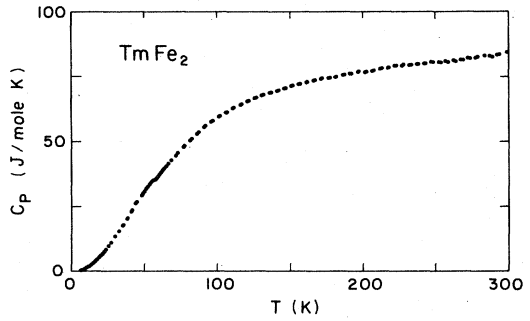

FIG. 30. Experimental heat-capacity data vs temperature for $TmFe_2$.

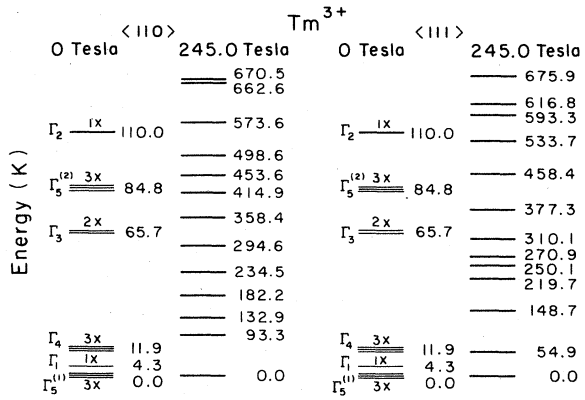

FIG. 32. Calculated energy level diagram for $TmFe_2$.

studies of Atzmony *et al.*[9] and Bowden *et al.*[20]

To obtain the best fit to the ΔC_p curve, the experimental data was fit in two regions. Below 50 K, the perturbing Hamiltonian with the crystal field interaction and exchange interaction in the ⟨110⟩ direction of magnetization was diagonalized with various combinations of B_4^0, B_6^0, and H_{exch}. The best fit in this region was obtained with the following parameters:

$$B_4^0 = (5.46 \pm 0.50) \times 10^{-3}\ \text{K}\ ,$$

$$B_6^0 = (3.54 \pm 0.30) \times 10^{-5}\ \text{K}\ ,$$

$$H_{\text{exch}} = 245 \pm 25\ \text{T}\ .$$

The transition occurs over $\sim 10°$, therefore the fit to the high-temperature region was initiated at 60 K. The Hamiltonian with the appropriate interactions in the ⟨111⟩ direction was diagonalized and the best fit to this region was obtained with the following parameters:

$$B_4^0 = (5.46 \pm 0.50) \times 10^{-3}\ \text{K}\ ,$$

$$B_6^0 = (3.54 \pm 0.30) \times 10^{-5}\ \text{K}\ ,$$

$$H_{\text{exch}} = 245 \pm 25\ \text{T}\ .$$

These parameters are identical to those obtained in the ⟨110⟩ direction. This is entirely expected. Because the easy axis of magnetization is determined by the magnetocrystalline free energy, one can only confirm that a direction is favored at a given temperature if the fit conditions remain constant throughout the temperature range. The direction with the lowest magnetocrystalline free energy at a given temperature under the same conditions determines the easy axis of magnetization.

Bowden *et al.*[20] predicted that the signs of B_4^0 and B_6^0 should be positive, as is the case. The ratio of A_6^0/A_4^0 is $-0.055 a_0^{-2}$. The energy level diagrams obtained from the fit of the ΔC_p data are given in Fig. 32.

Figure 33 illustrates the behavior of the calculated magnetocrystalline free energies with temperature. Figure 34 is a magnification of the transition region illustrating that the ⟨110⟩ free energy is lowest until ~ 41 K, at which point the ⟨111⟩ direction is favored. As can be seen, there is an almost tangential crossover in free energies in the region of the ΔC_p transition. This transition temperature is somewhat lower than in the actual ΔC_p data. However,

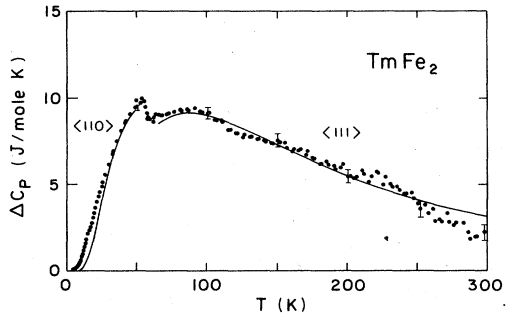

FIG. 31. ΔC_p vs temperature and calculated best fit curves for $TmFe_2$.

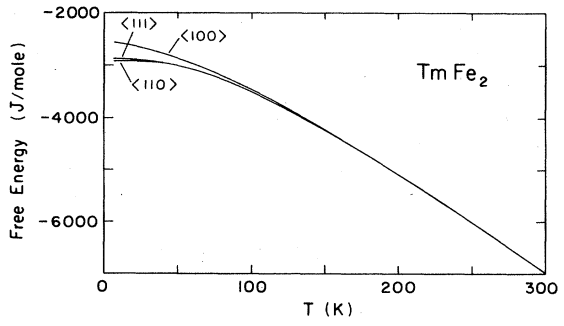

FIG. 33. Calculated magnetocrystalline free energies vs temperature for $TmFe_2$.

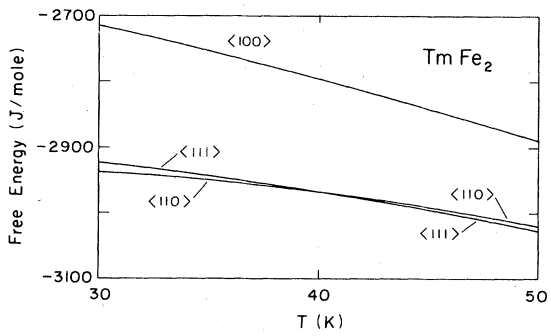

FIG. 34. Magnification of the magnetocrystalline free energies in the transition region for $TmFe_2$.

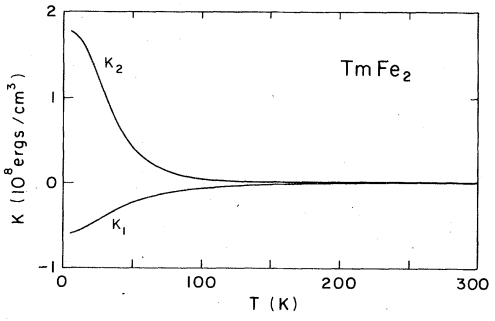

FIG. 36. Calculated bulk anisotropy constants vs temperature for $TmFe_2$.

errors of this magnitude are not unusual for calculated transition temperatures.[9] The important fact is that the calculated magnetocrystalline free energies in the $\langle 110 \rangle$ and $\langle 111 \rangle$ direction do cross near the experimental transition temperature, thus indicating a spin reorientation.

$\Delta S_{\text{expt}}/R \ln(2J+1) = 0.97$ at 300 K for $TmFe_2$. This is the largest contribution to the entropy of the entire series of RFe_2 compounds. Because the overall splitting of the energy levels is less than that of any member of the RFe_2 series and is of the order of 670 K, thermal excitation over the entire energy levels is nearly complete.

The behavior of the calculated Tm^{3+} moment is illustrated in Fig. 35. A break in the curve is evident at the calculated transition temperature of 41 K. Because the transition takes place over $\sim 10°$, the behavior of the moment from 35 to 45 K is not realistically represented by Fig. 35. The actual behavior of the moment at the transition would have to be determined by experiment.

The calculated value of σ at 0 K is $6.92\mu_B$ which is slightly less than that of the free ion, $g_J J = 7.0\mu_B$.

Neutron-diffraction studies by Rhyne[23] yield a σ value of $7.0\mu_B$ at 0 K. Only 40% of the 0 K calculated moment remains at 300 K indicating that $TmFe_2$ should exhibit the smallest magnetic anisotropy at room temperature of the RFe_2 series.

The calculated bulk anisotropy constants as a function of temperature are given in Figs. 36 and 37. When a direction other than $\langle 100 \rangle$ or $\langle 111 \rangle$ is favored, K_1 cannot be used to describe the easy axis of magnetization. As exhibited in the other RFe_2 compounds, the values of K_1 and K_2 are very large at 0 K in comparison to the 300 K values. The room-temperature values calculated by Dariel *et al.*[25] Atzmony *et al.*[9] and this work, Table V, are all the lowest encountered in the RFe_2 series as predicted by Clark[23]

I. $LuFe_2$

Figure 38 gives a plot of C_p vs T for $LuFe_2$. The $LuFe_2$ sample was used primarily for the determination of the heat-capacity blank, and the data are included here for completeness.

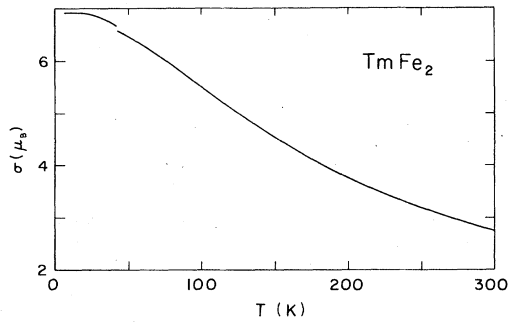

FIG. 35. Tm^{3+} calculated magnetic moment vs temperature for $TmFe_2$.

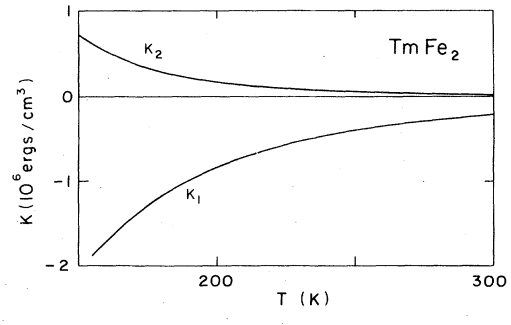

FIG. 37. Magnification of region in which the bulk anisotropy constants converge.

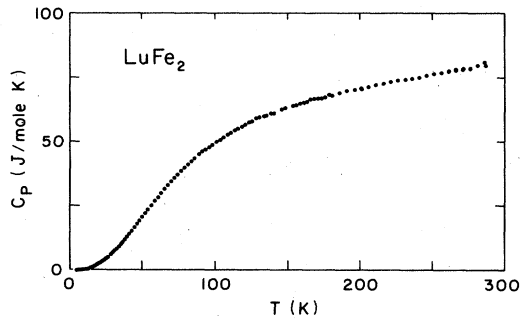

FIG. 38. Experimental heat-capacity data vs temperature for $LuFe_2$.

IV. SUMMARY

The results of a comprehensive investigation of the heat capacity of, and crystal field effects in, the RFe_2 compounds have been reported in this paper. Table VI summarizes the results and illustrates the trends apparent in the series.

The contribution to the heat capacity of $GdFe_2$ was unexpected but may be due to relativistic effects and mixing of higher state multiplets into the ground state. The transition in the $TmFe_2$ compound was fit under the assumption that it involved a spin rotation. However, neutron-diffraction studies would be necessary before the true nature of this transition can be determined.

ACKNOWLEDGMENTS

The authors wish to thank Dr. K. A. Gschneidner, Jr. for supplying the $LuFe_2$ sample used for the determination of the heat-capacity blank and also for very stimulating discussions with regard to this work. This work was in part supported by National Science Foundation Grant No. CHE 77/27252.

*Present address: Dow Chemical, Texas Division, Freeport, Tex. 77541.

[1]W. E. Wallace, *Rare Earth Intermetallics* (Academic, New York, 1973).

[2]A. E. Clark, in *Magnetism and Magnetic Materials—1973,* edited by C. D. Graham and J. J. Rhyne, AIP Conf. Proc. No. 18 (AIP, New York, 1974), p. 1015.

[3]N. C. Koon and J. J. Rhyne, Solid State Commun. 26, 537 (1978).

[4]K. H. J. Buschow and R. P. van Stapele, J. Appl. Phys. 41, 4066 (1970).

[5]D. J. Germano, R. A. Butera, S. G. Sankar, and K. A. Gschneidner, Jr., J. Appl. Phys., 50, 7495 (1979).

[6]C. Kunesh, Ph.D. thesis (University of Pittsburgh, 1970) (unpublished).

[7]D. J. Germano, Ph.D. thesis (University of Pittsburgh, 1980) (unpublished).

[7a]G. T. Furakawa, W. G. Saka, and M. L. Reilly, Report No. NSRDS-NBS 18 (unpublished).

[8]M. T. Hutchings, Solid State Phys. 16, 227 (1968).

[9]U. Atzmony, M. P. Dareil, E. R. Dauminger, D. Lebenbaum, I. Nowik, and S. Ofer, Phys. Rev. B 7, 4220 (1973).

[10]C. Deenadas, A. W. Thompson, R. S. Craig, and W. E. Wallace, J. Phys. Chem. Solids 32, 1853 (1971).

[11]R. A. Butera, T. J. Clinton, A. G. Moldovan, S. G. Sankar, and K. A. Gschneidner, Jr., J. Appl. Phys. 50, 7492 (1979).

[12]T. Knoue, S. G. Sankar, R. S. Craig, W. E. Wallace, and K. A. Gschneidner, Jr., J. Phys. Chem. Solids 38, 487 (1977).

[13]R. E. Hungsberg and K. A. Gschneidner, Jr., J. Phys. Chem. Solids 33, 401 (1972).

[14]T. Inoue, Ph.D. thesis (University of Pittsburgh, 1975) (unpublished).

[15]K. A. Gschneidner, Jr., in *Rare Earth Research,* edited by L. Eyring (Gordon and Breach, New York, 1965), p. 153.

[16]W. E. Wallace, S. G. Sankar, and V. U. S. Rao, Struct. Bonding, Berlin 33, 1 (1977).

[17]B. G. Wybourne, Phys. Rev. 148, 317 (1966).

[18]A. W. Thompson, Ph.D. thesis (University of Pittsburgh, 1971) (unpublished).

[19]R. Chatterjee, D. J. Newman, and D. C. Taylor, J. Phys. C 6, 706 (1973).

[20]G. J. Bowden, D. St. P. Bunbury, A. P. Guimaraes, and R. E. Synder, J. Phys. C 2, 1376 (1968).

[21]A. J. Freeman and R. E. Watson, in *Magnetism,* edited by G. J. Rado and H. Suhl (Academic, New York, 1965), Vol. II A, p. 292.

[22]K. R. Lea, M. J. M. Leask, and W. P. Wolf, J. Phys. Chem. 23, 1381 (1962).

[23]A. E. Clark, in *Handbook on the Physics and Chemistry of Rare Earths,* edited by K. A. Gschneidner, Jr., and L. Eyring (North-Holland, New York, 1979), Vol. 2, p. 242.

[24]A. E. Clark, J. R. Cullen, and K. Sato, in *Magnetism and Magnetic Materials—1974,* edited by C. D. Graham, G. H. Lander, and J. J. Rhyne, AIP Conf. Proc. No. 24 (AIP, New York, 1975), Vol. 24, p. 670.

[25]M. P. Dariel and U. Atzmony, Int. J. Magn. 4, 213 (1973).

[26]A. E. Clark, H. S. Belson, and N. Tamagawa, Phys. Lett. 42A, 160 (1962).

[27]E. Burzo, Solid State Commun. 14, 1295 (1974).

[28]U. Atzmony, in *Crystal Field Effects in Metals and Alloys,* edited by A. Furrer (Plenum, New York, 1977), p. 113.

[29]J. J. Rhyne and N. C. Koon, J. Appl. Phys. 49, 2133 (1978).

[30]J. J. Rhyne, N. C. Koon, J. B. Milstein, and H. A. Alperin, Physica 86, 149 (1977).

[31]R. L. Cohen, Phys. Rev. 134, A94 (1964).

[32]S. G. Sankar, S. K. Malik, and V. U. S. Rao, J. Solid State Chem. 18, 303 (1976).

[33]E. F. Westrum, Jr., and B. H. Justice, Phys. Chem. 67, 659 (1963).

[34]B. H. Justice and E. F. Westrum, Jr., J. Phys. Chem. 67, 345 (1963).

[35]B. H. Justice, E. F. Westrum, Jr., E. Chang, and R. Radebaugh, J. Phys. Chem. 78, 333 (1969).